Journal of Thermal Analysis and Calorimetry (2019) 138:1193–1205
https://doi.org/10.1007/s10973-019-08663-1

Thermal and spectroscopic studies on a double-salt-type pyridine–silver perchlorate complex having κ^1-O coordinated perchlorate ions

Berta Barta Holló[1] · Vladimir M. Petruševski[2] · Gréta Bettina Kovács[3,4] · Fernanda Paiva Franguelli[3,4] · Attila Farkas[5] · Alfréd Menyhárd[6] · György Lendvay[3] · István E. Sajó[7] · Laura Nagy-Bereczki[3] · R. P. Pawar[8] · Imre Miklós Szilágyi[4] · Eszter Bódis[3] · László Kótai[3,9]

Received: 26 June 2019 / Accepted: 31 July 2019 / Published online: 13 August 2019

Abstract

A simple synthetic method was developed to prepare $4[Agpy_2ClO_4]\cdot[Agpy_4]ClO_4$ in a low-temperature decomposition process of $[Agpy_4]ClO_4$. A detailed IR, Raman and far-IR study including factor group analysis has been performed, and the assignation of bands is given. The compound decomposes quickly with a multistep ligand loss process with the formation of $[Agpy_2]ClO_4$ and $AgClO_4$ intermediates and AgCl as an end product around ~ 85, ~ 350 and 450 °C, respectively. During the first decomposition step, a small fraction of the ligands is lost in a redox reaction: perchlorate oxidizes the pyridine, forming carbon, carbon dioxide, water and NO, while it itself is reduced into AgCl. In the next step, when $AgClO_4$ forms after complete ligand loss and reacts with the carbon formed in the degradation of pyridine at lower temperatures and produces NO, CO_2 and H_2O. This reaction becomes possible because the AgCl formed in the redox reactions makes a eutectic melt with $AgClO_4$ in situ, which is a favorable medium for the carbon oxidation reaction. AgCl is known to reduce the temperature of decomposition of $AgClO_4$, in which process forms AgCl as well as O_2 and so is an autocatalytic process. The loss and degradation of pyridine ligand are endothermic; the redox reactions including carbon oxidation and $AgClO_4$ decomposition into AgCl and O_2 are exothermic. The amount of absorbed/evolved heats corresponding to these processes was determined by DSC both under N_2 and O_2 atmospheres.

Keywords Pyridine–silver complexes · Perchlorates · Quasi-intramolecular solid-phase redox reaction · Evolved gas analysis · DSC

Electronic supplementary material The online version of this article (https://doi.org/10.1007/s10973-019-08663-1) contains supplementary material, which is available to authorized users.

✉ László Kótai
kotai.laszlo@ttk.mta.hu

[1] Department of Chemistry, Biochemistry and Environmental Protection, Faculty of Sciences, University of Novi Sad, TrgDositejaObradovića 3, Novi Sad 21000, Serbia

[2] Faculty of Natural Sciences and Mathematics, Ss. Cyril and Methodius University, Skopje, Republic of Macedonia

[3] Research Centre for Natural Sciences, Hungarian Academy of Sciences, Magyar Tudósok krt. 2, Budapest 1117, Hungary

[4] Department of Inorganic and Analytical Chemistry, Budapest University of Technology and Economics, Műegyetem rakpart 3, Budapest 1111, Hungary

[5] Department of Organic Chemistry, Budapest University of Technology and Economics, Budapest, Hungary

[6] Department of Physical Chemistry and Materials Science, Budapest University of Technology and Economics, Budapest, Hungary

[7] János Szentágothai Research Centre, University of Pécs, Ifjúságútja 20, Pecs 7624, Hungary

[8] Department of Chemistry, Deogiri College, Station Road, Aurangabad, MS 431005, India

[9] Deuton-X Ltd., Selmeci u. 89, Érd 2030, Hungary

Introduction

The pyridine–silver complexes are widely used in science and industry: as catalysts, oxidants and explosives [1–5]. Some of the numerous possible compounds of this class can be synthesized easily, and some of the properties of a few of them have been studied [6, 7]. Thus, when silver perchlorate ($AgClO_4$) is dissolved in pyridine (py), various complexes are formed: $4[Ag(py)_2ClO_4]\cdot[Ag(py)_4]ClO_4$ (compound **1**), $[Ag(py)_2]ClO_4$ (compound **2**), $[Ag(py)_2]ClO_4\cdot 0.5py$ (compound **3**) and $[Ag(py)_4]ClO_4$ (compound **4**) [8]. The phase diagram of the $AgClO_4$–pyridine–water system was also studied in detail and predicted by the formation of two compounds, compounds **2** and **3**, and a phase characterized by the formula $Ag_5py_9(ClO_4)_5$ was also detected [9]. The latter compound was later shown to be compound **1** with some pyridine deficiency, the latter caused by the easy loss of pyridine even at room temperature, analogously to that observed for the analogous permanganate compounds, $4[Ag(py)_2MnO_4]\cdot[Ag(py)_4]MnO_4$ (compound **1-MnO_4**) and $Ag_5py_9(MnO_4)_5$ [8, 10].

A detailed knowledge of the properties of pyridine–silver complexes, in particular of their thermal behavior, could widen the range of applications of these compounds [11]. The available information about the properties of the known pyridine–silver perchlorate complexes, however, is scarce. For example, while bis(pyridine)silver(I) perchlorate (compound **2**) has been known for a long time [12], all that is known is its crystal structure [13] and IR spectrum [8, 14], just as for $4[Agpy_2ClO_4][Ag(py)_4]ClO_4$, compound **1**, which was discovered during crystallization experiments of compound **2** [8, 14, 15]. For $[Ag(py)_4]ClO_4$, compound **3**, prepared first by Wilke-Dörfurt and co-workers [14] only the crystal structure is available [16]. The thermal behavior characterizing the stability and reactivity or the UV and Raman spectra of compounds **1–4,** however, have not been studied at all. This prompted us to perform a systematic study on the thermal and spectroscopic properties of the pyridine–silver(I) perchlorate complexes. In this work, we report on the thermal properties, IR, UV and Raman spectroscopic characteristics of compound **1** and compare it with the known permanganate analog $4[Ag(py)_2MnO_4]\cdot[Ag(py)_4]MnO_4$ (**1-MnO_4**) and some other pyridine–silver(I) perchlorate compounds listed in Table 1.

In the rest of this paper, a detailed thermal and spectroscopical characterization of compound **1** ($4[Agpy_2ClO_4][Ag(py)_4]ClO_4$) and its decomposition products is described.

Table 1 Composition and label of the compounds studied in this work

Compound	Label
$4[Ag(py)_2ClO_4]\cdot[Ag(py)_4]ClO_4$	**1**
$[Ag(py)_2]ClO_4$	**2**
$[Ag(py)_4]ClO_4$	**3**
$[Ag(py)_2]ClO_4\cdot 0.5py$	**4**
Decomposition intermediate from compound **1** at 85 °C	**DI-85**
Decomposition intermediate from compound **1** at 350 °C	**DI-350**
Decomposition product from compound **1** at 500 °C	**DP-500**

Experimental

Chemical-grade silver sulfate, pyridine and sodium perchlorate monohydrate and bidistilled water (Deuton-X Ltd., Hungary) were used. Several drops of pyridine were added to 200 mL water, and 0.8 g of Ag_2SO_4 was dissolved in it. Sodium perchlorate monohydrate (0.674 g) was dissolved in water (24 mL); then, this solution and 200 mL of 20% pyridine solution were added to the silver sulfate solution. The mixture was kept in an ice bath for several hours, and the formed white precipitate was filtered with suction and kept in a refrigerator for 10–14 days at 5–8 °C in an open crucible.

Vibrational spectroscopy

The FT-IR spectrum of solid compound **1** was recorded in the attenuated total reflection (ATR) mode on a Bruker Alpha IR and a BioRad-Digilab FTS-30-FIR spectrometer in the 4000–400 and 700–40 cm^{-1} range, respectively.

The Raman measurement of compound **1** was performed using a Horiba Jobin–Yvon LabRAM-type microspectrometer (external 532 nm and 785 nm Nd-YAG and diode laser source, respectively, ~ 40 mW, supplied with an Olympus BX-40 optical microscope). The 532 nm wavelength was used to make the low-temperature measurements (at − 20 and − 150 °C) using a Linkam THMS600 temperature-controlled microscope stage, while the spectrum at 785 nm was recorded at room temperature. The laser beam was focused by an objective of 20×, and a D0.6 (− 150 °C), D2 (− 20 °C) and D0.3 (room temp.) intensity filters were used to decrease the laser power to 25, 1 and 50%, respectively, in order to avoid the thermal degradation of the sample. The confocal hole of 1000 μm and 950 or 1800 groove mm^{-1} grating monochromators were used in a confocal system and for light dispersion depending on the laser source. The spectral range of 100–4000 cm^{-1} was detected with 3 cm^{-1} resolution. The exposure times were 15, 10 and 100 s at 25, − 150 and

− 20 °C, respectively, to obtain intensive peaks at the applied conditions.

UV–Vis spectroscopy

The diffuse reflectance spectrum of compound **1** (in solid phase) in the UV–Vis region was detected at room temperature by a Jasco V-670 spectrophotometer equipped with NV-470-type integrating sphere (using an official $BaSO_4$ standard as reference).

Powder X-ray diffractometry

X-ray powder diffraction measurements were taken using a Philips PW-1050 Bragg–Brentano parafocusing goniometer equipped with a Cu cathode operated at 40 kV and 35 mA tube power, with a secondary beam graphite monochromator and a proportional counter. Scans were recorded in step mode. The diffraction patterns were evaluated by full-profile fitting techniques.

Thermal studies

Thermal data were collected using TA Instruments SDT Q600 thermal analyzer coupled to Hiden Analytical HPR20/QIC mass spectrometer. The decomposition was followed from room temperature to 500 °C at 5 °C min^{-1} heating rate in argon carrier gas (flow rate = 30 cm^3 min^{-1}) and at 2 °C min^{-1} heating rate in air carrier gas (flow rate = 30 cm^3 min^{-1}). Sample holder/reference is alumina crucible/empty alumina crucible. Sample mass ~ 1 mg. Selected ions between m/z = 1–101 were monitored in multiple ion detection modes (MIDs).

The non-isothermal DSC curves were recorded between − 150 and 30 °C using a PerkinElmer Diamond DSC apparatus under N_2 with 5 °C min^{-1} heating rate supplied with two cooling systems (liq. N_2 and intracooler (− 85 °C). The decomposition processes were monitored both in N_2 and in O_2 atmospheres, using a PerkinElmer Diamond instrument with intercooler, between − 30 and 400 and using a PerkinElmer STA6000 simultaneous TG/DTA instrument between 30 and 500 °C, respectively. The heating rates were 5 °C min^{-1} under N_2 and 2 °C min^{-1} under O_2 until 200 °C and 5° min^{-1} between 200 and 500 °C. Sample masses were between 3 and 5 mg under continuous gas flow (20 cm^3 min^{-1}) in an unsealed aluminum pan.

CHN content

The carbon, hydrogen and nitrogen contents were measured by standard automatized elemental analysis (Fisons model CHN 1018S). The silver content of the sample was determined by atomic emission spectroscopy using a Spectro Genesis ICP-OES (SPECTRO Analytical Instruments GmbH, Kleve, Germany) simultaneous spectrometer with axial plasma observation. A multielement standard solution (Merck Chemicals GmbH, Darmstadt, Germany) was used for calibration.

Identification of decomposition intermediates

The final products of the thermal decomposition products were formed as a glassy material and proved to be mechanically unrecoverable from the surface of the ceramic boat. Therefore, to identify the product, the boat was immersed in an ammonia solution (25 mass%) for an hour, and the formed solution was acidified with HNO_3. A white precipitate was formed, which was filtered off, dried at 105 °C and identified by XRD.

The decomposition intermediate formed at 350 °C proved to be a sticky material, which could not be removed mechanically from the boat surface, either. This material was also dissolved in 25% aq. ammonia; then, the solvent was evaporated to dryness in a desiccator at room temperature. The formed crystalline mass was identified based on its IR spectrum and XRD patterns.

The gases evolved during heating of 100 mg of a sample of compound **1** at 85 °C in a water bath with N_2 purging were introduced into water to absorb its pyridine content in it. The acidimetric determination of pyridine dissolved in the water, however, failed due to the formation of NO and CO_2 acidic gases. To detect the presence/absence of chloride ions, an acidified ($HClO_4$) 0.1 M $AgNO_3$ solution was used.

Results and discussion

Synthesis and structural features

Dyason and co-workers identified first the compound **1** as an intermediate formed during recrystallization of a multiphase mixture formed in the reaction of $AgNO_3$, pyridine and $NaClO_4$ [12] from 5:1 $CHCl_3$/pyridine mixture (v/v) and determined its crystal structure [15]. A more convenient way to isolate compound **1**, as well as three other compounds (**2**–**4**), was found in the studies on the $AgClO_4$–pyridine–H_2O system [8, 9]. In the present work, the method given in [8] was slightly modified to simplify the procedure. A mixture of pyridine–silver(I) perchlorates(-compounds **1** and **3**) was prepared from Ag_2SO_4, 20% aq. pyridine and 0.2 M aq. $NaClO_4$ at + 8 °C [8] and was kept at 5–8 °C in a fridge for 10–14 days in an open crucible. The transformation of compound **3** into compound **1** can be followed by XRD (ESI Fig. 1). Covering the crucible with

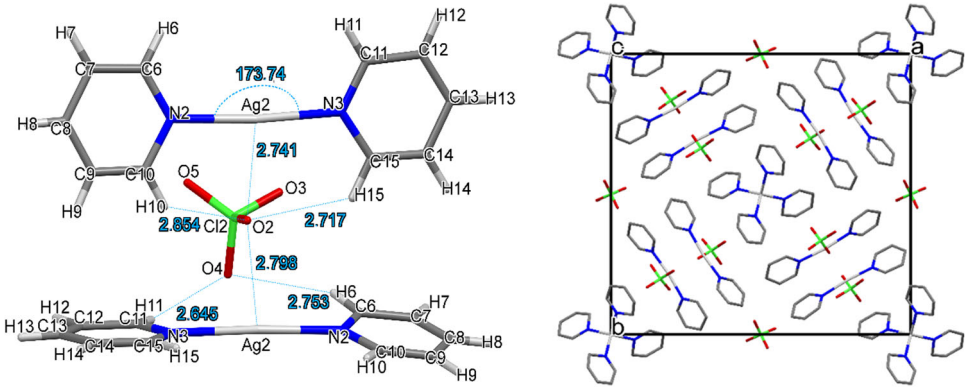

Fig. 1 Structural features and packing of compound **1** [15]

a foil and putting the sample to a deep freezer (− 20 °C), the composition of the mixture does not change for weeks.

Compound **1** was isolated as white crystals which quickly decompose at room temperature with intensive pyridine smell, forming $[Agpy_2]ClO_4$. Although compound **1** is less stable than compound **2** (T_{dec} = 68 °C vs. 158.6 °C [8, 9]), it was found to be stable in the dry state below + 8 °C in a closed vessel for weeks.

The double salt **1** crystallizes in the tetragonal crystal system (space group I-4, Fig. 1). It is isomorphous with the permanganate analog [17]. The unit cell volume of **1** is 0.85% larger than that of compound **1-MnO$_4$**; their cell similarity index (π) [18] is 0.00044.[1]

There is one $[Ag(py)_2ClO_4]$ and one-quarter of $[Ag(py)_4]ClO_4$ in the asymmetric unit. The Kitaigorodskii packing coefficient [19] is 67.6%, and there is no residual solvent-accessible void in the crystal lattice. The pyridine rings are rotated by an angle of 13.4° with respect to each other [15]. This is larger than in the analogous permanganate **1-MnO$_4$** (12.03°) [16]. The C_α–H…O–XO_3 interactions in the compound **1** (X = Cl) are stronger than in the permanganate analog (X = Mn), the C_α…O distance being 2.645 Å and 3.121 Å in compounds **1** and **1-MnO$_4$**, respectively. The $[Agpy_2ClO_4]$ units form chains along the *c* crystallographic axis. The silver–silver distance between the $[Agpy_2ClO_4]$ units in compound **1** is 4.843 Å, which is larger than that in compound **2** (2.999 Å) and much larger than the sum of the van der Waals radii of two Ag atoms, 3.44 Å [20, 21]. Thus, in compound **1**, there is not even a week argentophilic interaction. The shortest Ag…O–ClO_3 distance is 2.740 Å. This distance is shorter than the sum of the covalent radii of silver (1.33 Å) [22] and the non-bonded radius of oxygen (1.5 Å) [20, 23], the shorter than 2.83 Å, which is a sign of a non-negligible, albeit weak Ag to perchlorate interaction. Comparison of the Ag…O–ClO_3 distance in compound 1 with the Ag…O–MnO_3 distance in **1-MnO$_4$** (2.601 Å) indicates that the coordination strength of the perchlorate to the silver ion is weaker than that of the permanganate. The deviation of the N–Ag–N angle from the ideal 180° is somewhat larger in the perchlorate (6.26°) [15] than in the permanganate (6.15°) [17].

The geometry of the $[Ag(py)_4]^+$ ion is tetrahedral; the Ag^+ cation is placed on a $\bar{4}$ inversion axis. The $[Ag(py)_2ClO_4]$ chain and the $[Ag(py)_4]^+$ cations are connected by Cl–O…π interactions, where the Cl–O…C_g(py) distance is 3.599 Å [15]. This is longer than the corresponding value in the analogous permanganate complex (3.469 Å) [17], suggesting that the strength of the interaction of the perchlorate to pyridine is also weaker than that of the permanganate ion, similarly to the anion–Ag^+ interaction.

Compound **1** has no polymorphic phase transition between − 150 °C and its decomposition temperature.

Vibrational spectroscopic results of compound 1

Vibrational modes of the coordinated/non-coordinated perchlorate ions

The far-IR spectra of compound **1** were studied by Bowmaker and coworkers [14]; the assignations and the separation of Ag–N bands characterizing the$[Agpy_2]$ and $[Agpy_4]$ units were also performed. No detailed Raman data are available characterizing vibrations of the perchlorate ion in these compounds. Correlation diagrams for ClO_4^- anions at S_4 (free-standing non-coordinated perchlorate ion) and C_1 (perchlorate coordinated to the $[Ag(py)_2]^+$ cation) sites of compound **1** lattice are presented in Fig. 1. We recorded the IR and Raman spectra of compound 1. The room-temperature Raman spectrum is shown in Fig. 3; the mid-IR and far-IR spectra are presented in ESI Figures 2 and 3, respectively. The observed IR and Raman frequencies and their assignations are collected in Table 2.

There are nine internal modes of the ClO_4^- anions at both positions. At S_4 sites, two modes of the factor group (f–g) (*B* and *E* symmetry) are IR active, whereas all f–g modes (*A*, *B* and *E* symmetry) are Raman active. At C_1

[1] Cell similarity index: $\pi = |(a+b+c)/(a'+b'+c') - 1|$.

Table 2 IR and Raman wavenumbers of perchlorate ion vibrations in compound **1** at room temperature

IR, 25 °C	Raman bands at 25 °C (785 nm) and low-temperature excitations (532 nm)			Assignation
	25 °C	− 20 °C	− 150 °C	
944	911 (w)	907 (w)	908 (w)	ν_1(ClO), ν_s(A)
–	928 (m)	926 (m)	927 (m)	
462 (w)	460 (w)	456 (w)	457 (w)	ν_2(ClO), δ_s(E)
415 (w)	417 (w)[a]	412(vw)[a]	414 (vw)[a]	
1154 (w)	1157 (w)	1155 (w)	1155 (w)	ν_3(ClO) ν_{as}(F_2)
1122 (sh)	1121 (vw)	1118 (vw)	1118 (vw)	
1079 (vs)	1099 (vw)	1096 (vw)	1096 (vw)	
1064 8vs)	1073 (vw)	1071 (vw)	1072 (vw)	
1034 (m)	1037 (w)	1035 (w)	1034 (w)	
651 (vw)	651 (w)	649 (w)	649 (w)	ν_4(ClO), δ_{as}(F_2)
635 (w)	632 (vw)	630 (vw)	631(vw)	
618 (m)	622 (w)	620 (w)	620 (w)	

vs very strong, *s* strong, *m* medium, *w* weak, *vw* very weak

[a]These bands may belong to coordinated pyridine modes as well

sites, each mode from the site group splits into three components in the factor group; thus, there are 9*A*, 9*B* and 9 *E* modes (*E* modes are doubly degenerate) giving rise to 36 vibrational degrees of freedom due to the 4 ClO_4^- anions on general positions (C_1 symmetry). There are six external vibrations of the perchlorate anions at S_4 sites; 3 and 4 bands are expected in the far-IR and the low-frequency part of the Raman spectra, respectively. The external vibrations of the perchlorate anions at C_1 sites result in 24 vibrational degrees of freedom due to four perchlorate anions on general symmetry positions. No predictions of the band intensities can a priori be given. The symmetric stretching mode of the Cl–O bond (ν_1, A_1) in the Raman spectrum is located at around 911 and 928 cm^{-1}, as medium and weak bands belong to perchlorates at S_4 and C_1 sites. Shifts to lower wavenumbers were observed at cooling to − 20 or − 150 °C without any splitting of the band system. In the IR spectrum, the band that appears and shifts to 944 cm^{-1} probably belongs to the coordinated perchlorate ion, because the IR-forbidden band appears in the case of C_1 perchlorates due to pronounced distortion [23, 24]. For a "free" perchlorate ion, this band does not appear in the IR spectrum, because it is forbidden by the selection rules (Fig. 2).

The ν_2(E) bands (symmetric deformation mode) should appear as two doublets, but a singlet (459 cm^{-1}) and a doublet (460 and 417 cm^{-1}) were found in the IR and Raman spectra, respectively. The intensities of the two bands in the Raman spectra are different. The higher wavenumber bands belong to the coordinated perchlorate (C_1 site), while the lower-frequency band might be due to ν_2 mode of the perchlorate located at the S_4 site, but may also belong to a coordinated pyridine mode [14] as well. The wavenumbers and intensities of bands in the Raman spectra become smaller with the decrease in the temperature of the measurement. The Raman spectrum at room temperature is given in Fig. 3, while the low-temperature Raman spectra (− 25 and − 150 °C) are given in ESI Figures 4 and 5, respectively.

There are five Raman and four IR bands in the range of ν_3 (F_2) asymmetric Cl–O stretching bands (1157–1035 cm^{-1}), which could be assigned to result from two triplets, which partly overlap each other resulting in five weak bands in the Raman spectrum and two very intensive and two weak bands in the IR spectrum. The splitting of triply degenerate modes could be the consequences of the pronounced distortion [24, 25] due to the coordination of perchlorate to silver, but the two intensive bands may also belong to the two types (C_1 and S_4) of perchlorates. The almost same intensity, and the shoulder on the left side of the higher wavelength intense band, however, strongly suggests that these intense bands belong to the same type of perchlorate (the coordinated one), and the weaker intensity bands belong to the four times fewer non-coordinated (S_4 type) anions. The situation is complicated enough because some of the pyridine modes are located in this spectral range (ν_7 and ν_8, A_1 in-plane CH_{wag} and ring bendings at 1071 and 1031 cm^{-1}; ν_{26} B_2 in-plane CH_{wag} at 1068 cm^{-1}—the symmetry species A_1 and B_1 refer to the C_{2v} symmetry of free pyridine), which may also be part of the multiple band system. Taking into consideration that the ν_3(F_2) bands of tetrahedral ions are very intense bands in the IR and relatively weak bands in the Raman spectra, the bands at 1064/1079 cm^{-1} (IR) and

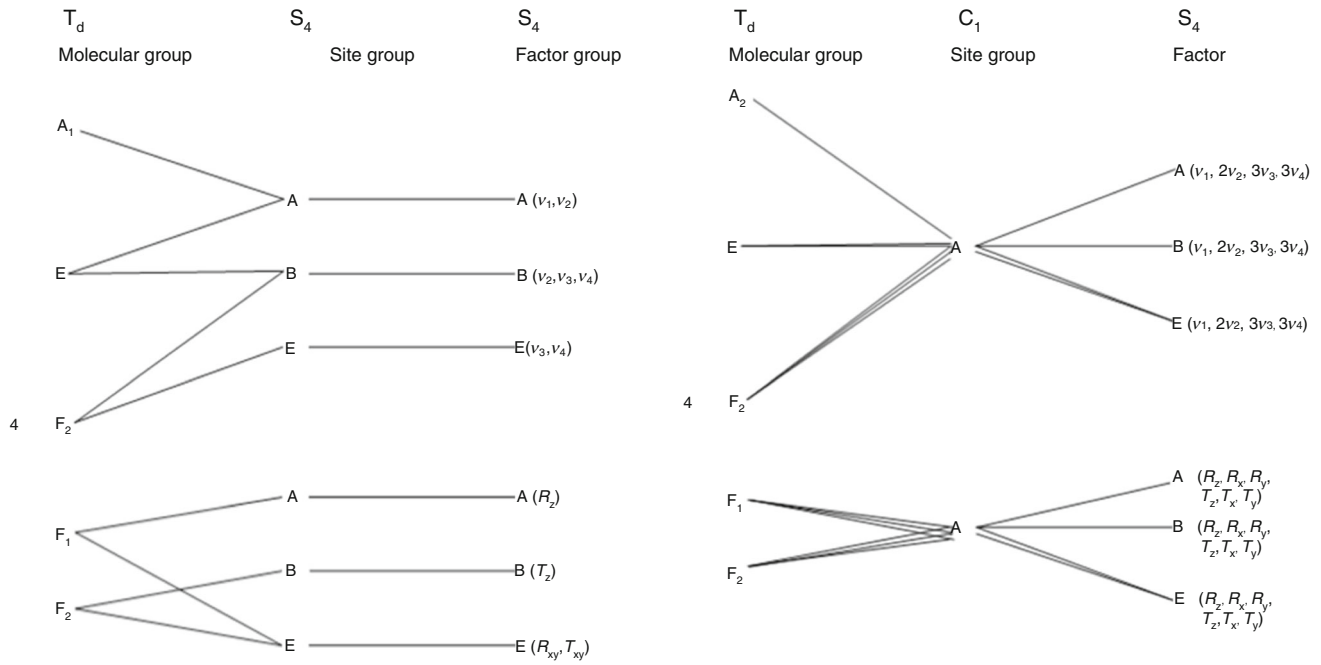

Fig. 2 Correlation diagram for perchlorate anions in the lattice of $4[Agpy_2ClO_4]$ $[Agpy_4]ClO_4$ at S_4 (**a**) and C_1 (**b**) sites. *R* and *T* mark hindered rotations and translations of the perchlorate anions, respectively

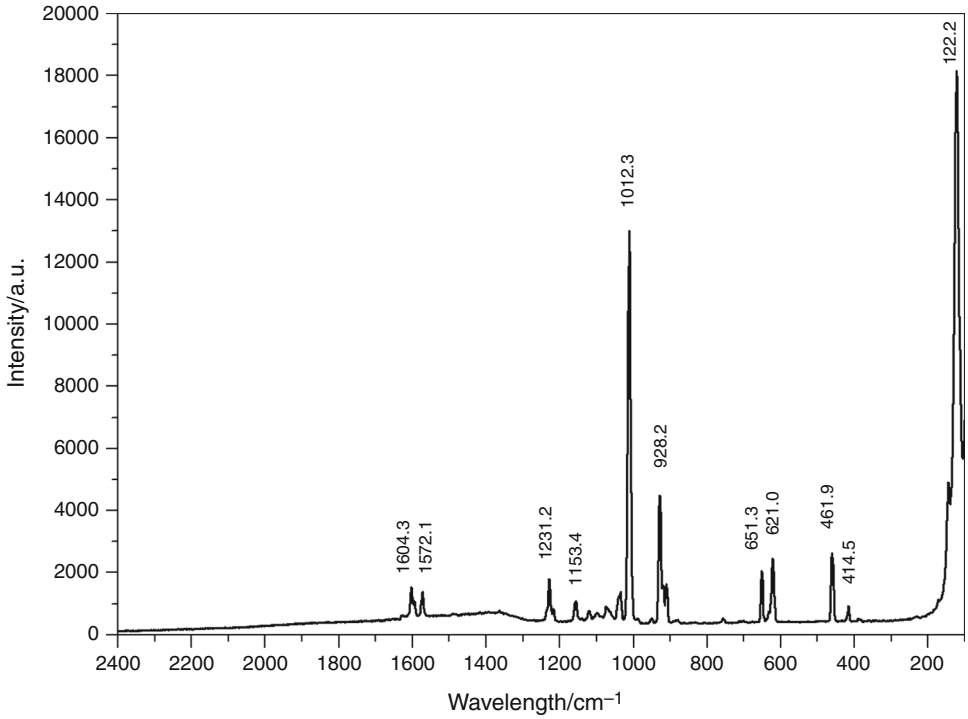

Fig. 3 Raman spectrum of compound **1** at room temperature

1071/1099 cm^{-1} (Raman) could be assigned as originating from the coordinated perchlorate modes. The other bands may belong to S_4-type perchlorate or pyridine modes.

The fourth normal mode, the $\nu_4(F_2)$, asymmetric deformation bands appear as triplets in both Raman and IR spectra. The lower Raman band component around 622 cm^{-1} and the 617 cm^{-1}in the IR spectrum belongs to the A_1 component of the split (A_1 + E according to the C_{3v} symmetry lowering) F_2 mode. The other, basically doubly degenerate components around 651 cm^{-1} appear in both

IR and Raman spectra and may be taken as an indicator of the monodentate (C_{3v}) perchlorate coordination [26]. This band at 651 cm^{-1}, however, may be overlapped with the v_{27} band of the pyridine (B_2 in-plane ring bending) as well. The third very weak band may be a combination band of low-frequency modes or a component of the split E mode due to further symmetry lowering into C_s due to hydrogen bonds between the perchlorate oxygens and pyridine α-CHs (Fig. 1) [14].

The distinction of the v_1–v_4 bands belonging to S_4 and C_1 sites is challenging. The coordination causes shifts of the Cl–O bands toward higher wavelengths. The amount of two types of perchlorates (C_1 and S_4), however, results in an expected ∼ 4:1 intensity ratio for the same mode, influenced by the coordination of perchlorate at C_1 sites as well, of course. Based on the well-defined v_1(Raman) and v_3(IR) bands pairs belonging to the two types of perchlorates, the bands with the higher intensities within the pairs probably belong to the coordinated perchlorates (C_1 site).

Assigned cation vibration modes of compound 1

There are two sets of cation vibrations ($[Ag(py)_2]^+$ and $[Ag(py)_4]^+$) arising from the hindered Ag translations within the cationic units. The correlation diagrams for the translations of Ag^+ cations at S_4 and C_1 sites are given in ESI Figure 6. A total of 3 and 12 vibrational degrees of freedom exist for S_4 and C_1 sites, respectively. All f–g modes and only *B* and *E* modes are active in Raman and IR, respectively. The 27 internal vibrational modes of the coordinated pyridine rings at C_1 sites split into 3–3 components in the factor group (27A, 27B and 27E), and because of double degeneracy of the 27 *E* modes, they give rise to 108 vibrational degrees of freedom. The three types of pyridine rings result in 324 vibrational modes of freedom corresponding to internal vibrations of the coordinated pyridine molecules. Each mode of external vibrations from the site group splits into three components in the factor group. There are 6 *A*, 6 *B* and 6 *E* (doubly degenerate) modes giving rise to 24 vibrational degrees of freedom. Due to three types of pyridine rings, there are 72 vibrational modes of freedom corresponding to external vibrations of the pyridine molecules.

Based on our Raman and IR and Bowmaker's [14] far-IR studies, the re-assignments of Ag–N vibrations belonging to $[Ag(py)_2]^+$ and $[Ag(py)_4]^+$ cations in compound **1** are given in Table 3. The IR frequencies of the tetrahedrally coordinated $[Ag(py)_4]^+$ cations differ from those of the $[Ag(py)_2]^+$ which are consistent with the variations of the Ag–pyridine bond strength (distance) and the increasing coordination number in the complexes. The bond lengths in $Agpy_2^+$ and $Agpy_4^+$ units are 2.15 Å and 2.30 Å [15], respectively; thus, the wavenumbers for the tetrahedrally coordinated species are expected to be lower than the values of $[Agpy_2]^+$ cation. The two bands in the far-IR spectrum at ∼ 228 and 164 cm^{-1} are assigned as v_s and v_{as} modes of $Agpy_2^+$ cation in compound **1.** The band at 136 cm^{-1} may belong to v_{as} (AgN in $Agpy_4$). In the Raman spectrum, the asymmetric AgN mode of $Agpy_2^+$-cation (172 cm^{-1}) and the high-intensity band at 122 cm^{-1} together with the weak one at 144 cm^{-1} could be found. The last two peaks were assigned as v_s and v_{as} modes of $Agpy_4^+$ cation. The higher intensity of symmetric stretchings than its asymmetric pair in the Raman spectra of tetrahedral anions has a diagnostic value in identifying the $v_1(A_1)$ mode.

Vibrational modes of the pyridine ligand

The factor group analysis results are given in ESI Fig. 7. The coordinated pyridine bands at 412 and 419 cm^{-1} for compound **1** [14] (412 and 418 cm^{-1} for compound **1-MnO_4**) [17] belong to coordinated pyridine modes of the $[Ag(py)_2]^+$ and the $[Ag(py)_4]^+$ cations, respectively. The appearance of single bands for $[Ag(py)_2]ClO_4$ at 412 cm^{-1} and for $[Ag(py)_4](ClO_4)$ at 419 cm^{-1} confirms these assignations [8, 15].

Table 3 IR and Raman wavenumbers of cations vibrations in compound **1** at room temperature

IR, 25 °C	Raman bands at 25 °C (785 nm) and low-temperature excitations (532 nm)			Reference data [14]	Assignation
	25 °C	− 20 °C	− 150 °C		
228 (vw)	–	–	–	245 (IR)	v_s(AgN) in $Agpy_2^+$
164 (w)	172 (vw)	166 (sh)	169 (vw)	166 (IR)	v_{as}(AgN) in $Agpy_2^+$
∼ 136 (vw)	144 (w)	140 (sh)	143 (w)	145 (IR)	v_{as}(AgN)
–	122 (vs)	115 (s)	119 (m)	122 (IR)	v_s(AgN) (our), v_{as}(AgN) [14]
	Out of our measurement range			88 (Raman)	v_s(AgN) [14]

vs very strong, *s* strong, *m* medium, *w* weak, *vw* very weak

[a]These bands may belong to coordinated pyridine modes as well

The derivation of the Raman spectra showed that the band at 417 cm^{-1} consists of two maxima, one at 411 and the other at 421 cm^{-1}. Although the v_2 mode of perchlorate may also be a doublet, the two components of the band at 417 cm^{-1} may also belong to the Ag–pyridine coordination for the $Agpy_2^+$ and $Agpy_4^+$ cations [14], respectively. The assignment of the overlapped bands belonging to the pyridine ligand is given in ESI Table 1.

UV–VIS spectra of compound 1

The perchlorate ion is UV silent [26]; thus, the diffuse reflection UV–Vis spectrum of compound **1** contains only a band system consisting of pyridine *n*-π^* and Ag^+–pyridine MLCT bands [8, 27, 28] (ESI Figure 8). Since Ag^+ is a d^{10} ion, no *d*–*d* transitions occur. The band maxima and their assignations are shown in Table 4.

The number of bands belonging to each transition of compound **1** is multiplied due to the presence of two kinds of pyridine containing complex cations ($[Ag(py)_2]^+$ and $[Ag(py)_4]^+$). The 218.9 and 295.2 nm bands may be assigned as frequencies for CT band, whereas the 251.5 nm band is the component of the pyridine ($^1A_{1g}$–$^1B_{2u}$ ($\pi \rightarrow \pi^*$)) transition [27, 28]. These bands are close to those found for $[Ag(py)_2]NO_3$ (219.4, 291.0 and 252.2 nm, respectively) [17] (Table 4).

Unique features in the thermal decomposition of compound 1

The thermal decomposition of **1** shows a remarkable complexity. In addition to the obvious ligand loss leading to the formation of silver perchlorate, additional reactions are possible because the anion is an oxidant and the ligand is oxidizable. When such oxidation reactions take place in the solid phase, gas-phase oxidation products, namely oxides of C, N, H as well as solid carbon, can be formed, while the residue of perchlorate is chloride, i.e., the by-product of the ion will be AgCl. The appearance of the latter can lead to additional reactions: it forms a eutectic with the $AgClO_4$ formed in the "regular" ligand loss, and it is also known to catalyze the decomposition of the perchlorate. In the following, we describe in detail the investigations of the thermal behavior of **1**, from which we derive the reaction scheme characterizing the decomposition and the formation of various products in different stages of the decomposition.

The thermal characteristics of **1** were studied by TG–MS in the dynamic atmosphere of both argon and synthetic air. As pre-experiments for planning DSC measurements, later simultaneous TGA–DTA curves of **1** were also recorded in N_2 and O_2. Here we discuss the thermogravimetric properties of **1** first in Ar and then in air, followed by the analysis of TG–DTA curves measured under N_2 and O_2.

The thermal decomposition of **1** in argon begins somewhat above room temperature at about 45 °C (Fig. 4) with loss of two molecules of pyridine. The first mass loss of 8.5% (DTG maximum at 77 °C) is close to but somewhat higher than that corresponding to two pyridine molecules (7.96%). This confirms that a part of the residual pyridine and perchlorate ions were also degraded. The overall process is endothermic.

The TG and DTG curves have shown that the intermediate after the loss of two pyridines (denoted as **DI-85**) is stable and it is possible to isolate. To identify the decomposition intermediate **DI-85**, we prepared it by isotherm heating of **1** at 85 °C for 1 h in N_2. XRD showed that it is $[Agpy_2]ClO_4$(compound **2**) (ESI Figure 10). Neither reduction products of perchlorate ion, i.e., AgCl in the solid residue (XRD), nor HCl in the gas phase could be detected. It shows that the amount of AgCl is below the detection limit of XRD. The intermediate $[Ag(py)_2]ClO_4$ (compound **2, DI-85**) is stable up to 105 °C. Further degradation/release of the rest of the pyridine ligands can be observed above this temperature. Several processes take place simultaneously as witnessed by numerous overlapping peaks in the DTG curves. Due to overlapping processes, no stable and pure intermediates could be isolated in the studied temperature interval from 105 up to ~ 300 °C. The mass loss was found to be 42.6% between 105 and 305 °C, a bit higher than that calculated for loss of 10 mol of pyridine from one mole of compound **1** (39.8%). The difference between the calculated and found mass loss suggests that some side reactions occur and form gaseous products.

DI-350 intermediate was prepared by isotherm heating of **1** at 350 °C for 0.5 h in N_2. The product was sticky and glassy and could not be removed mechanically from the ceramic crucible. Therefore, it was dissolved in cc. NH_3 solution and the solvent were left to evaporate at room

Table 4 UV spectral data of compound **1**

Compound/band	Compound 1	Compound 1-MnO_4 [17]	$[Ag(py)_2]NO_3$
Ag-pyCT	218.9 and 295.2	219.9	219.1 and 291.0
Pyridine, $^1A_{1g}$-$^1B_{2u}$ ($\pi \rightarrow \pi^*$) (L_b)	251.5	258.4	252.2

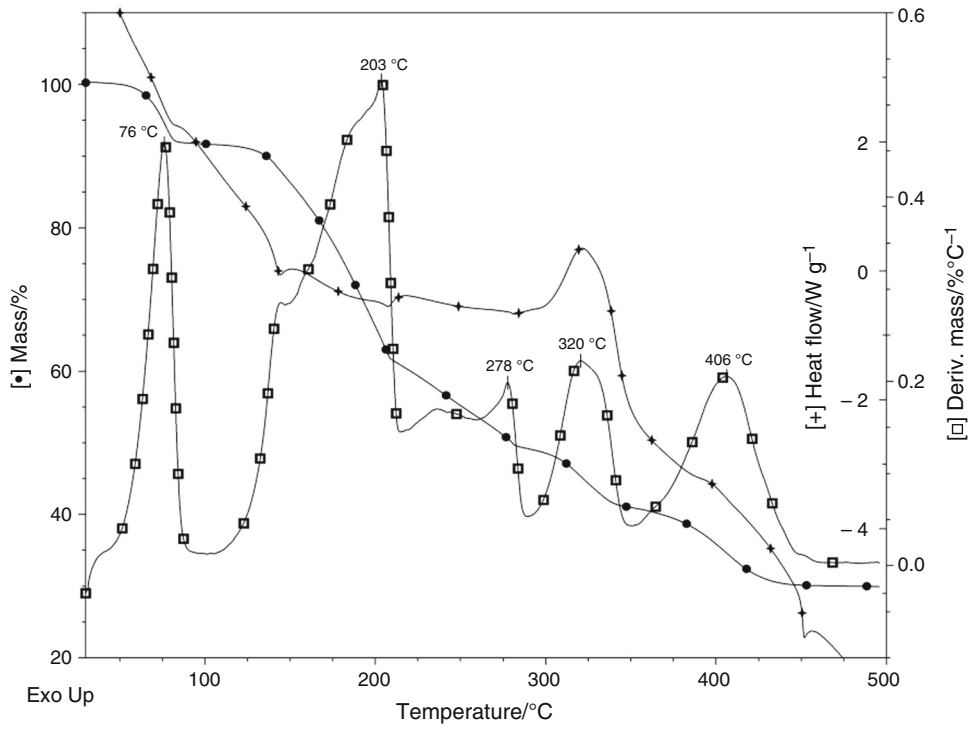

Fig. 4 Thermal curves of $4[Ag(py)_2ClO_4]\cdot[Ag(py)_4]ClO_4$ (**1**) in argon

temperature. In the IR spectrum (ESI Figure 11) of the solid residue, the bands of the diamminesilver cation[2] and of the perchlorate[3] could be assigned. The band positions agreed well with those of $[Ag(NH_3)_2]ClO_4$ [29].[4] The other N–H and Cl–O bands also strongly overlap with the corresponding bands of $[Ag(NH_3)_2]ClO_4$, and the $\rho_r(NH_3)$ of the $[Ag(NH_3)_2]ClO_4$ also coincides with the $\delta_{as}(ClO)$ bands [29, 30]. Since the main product of the dissolution of the **DI-350** in aqueous ammonia is $[Ag(NH_3)_2ClO_4$, the main component of **DI-350** can only be $AgClO_4$. We have not detected ammonium chloride, but NH_4ClO_4 was found.[5] The XRD study of this residue confirmed the presence of orthorhombic $[Ag(NH_3)_2ClO_4$, NH_4ClO_4, and some AgCl (ESI Figure 12).[6]

As we have seen above, compound **1** loses all pyridines at around 300 °C, and $AgClO_4$ is formed. At higher temperatures, $AgClO_4$ also decomposes. Two steps appear on the DTG curves with maxima at 347 and 425 °C. The expected product is AgCl. The residual mass of the end product is about 30% of the original weighting, which is somewhat less than the value calculated (36.09%). The mass deficit was found to be caused by a part of the facile evaporation of the AgCl [33]. There are two exothermic peaks on DTA with multiplet character (306.9 and 460.4 °C peak temperatures and 370.61 and 577.35 kJ mol^{-1}, respectively). The formation of AgCl accelerates the decomposition of $AgClO_4$, i.e., the decomposition process is autocatalytic [34]. It is worth mentioning that $AgClO_4$ and AgCl are known to form a eutectic melt (its melting point is 325 °C; those of $AgClO_4$ and AgCl are 476 and 451 °C, respectively) [34]. Since AgCl is formed in the redox reactions at lower temperatures, the eutectic can be formed as soon as $AgClO_4$ is formed in the decomposition of **1**.

To justify the identity of the final product of decomposition, it was prepared by isotherm heating of compound **1** at 450 °C. The process resulted in a glassy-like unremovable material, which was again bound strongly to the ceramic crucible and was unremovable mechanically. Treatment with ammonia produced $[Ag(NH_3)_2]Cl$. Acidification of the solution with HNO_3 resulted in dissolved NH_4NO_3 and a solid residue. This solid residue was filtered off and identified by XRD as AgCl (ESI Figure 13).

[2] IR bands of $[Ag(NH_3)_2]^+$ are: $\nu_{as}(NH)$ = 3286 cm^{-1}, $\nu_s(NH)$ = 3183 cm^{-1}, $\delta_{as}(NH)$ = 1612 cm^{-1}, $\delta_s(NH)$ = 1241 and 1213 cm^{-1}.

[3] IR bands of ClO_4^- are: $\nu_s(ClO)$ = 926 cm^{-1}, $\delta_s(ClO)$ = 453 cm^{-1}, $\nu_{as}(ClO)$ = 1055 cm^{-1} and $\delta_{as}(ClO)$ = 616 cm^{-1}.

[4] There are NH stretching bands at 3363 (ν_{as}(N–H)) and 3213 cm^{-1}, $\nu_s(NH)$; furthermore, the $\delta_s(NH)$ band also appears at 1417 cm^{-1}, and two perchlorate bands could be separated with relatively low intensity at 923 and 655 cm^{-1} [$\nu_s(ClO)$ and $\delta_{as}(ClO)$, respectively], which are close to the appropriate values found for NH_4ClO_4 [28].

[5] NH_4ClO_4 was formed due to a quasi-intramolecular acid–base reaction of diamminesilver(I) perchlorate [29, 30].

[6] The formation of AgCl during thermal decomposition of silver perchlorate is favored to that to the formation of Ag_2O [31]. Ammoniacal leaching converts AgCl into soluble $[Ag(NH_3)_2]Cl$. But during evaporation to dryness, the $[Ag(NH_3)_2Cl]$ loses its coordinated ammonia and transforms back into insoluble AgCl [32].

In the dynamic atmosphere of air, the decomposition steps of compound **1** are located at lower temperatures than in Ar (ESI Fig. 9). The mass losses were found to be higher than those found in the inert atmosphere, 9.8% (vs. 8.5%) in the first step and an additional 52.1% in the following one, taking place up to 300 °C, respectively. This is more than the total pyridine content in **1**; thus, decomposition of some other constituents needs to be assumed, for which the perchlorate groups are the only candidates. The enhanced mass loss in air as compared with that in inert atmosphere shows that the decomposition of perchlorate is more efficient when oxygen is present in the gas phase. This indicates that oxygen participates in some exothermic processes, which provides activation energy for perchlorate ($\sim$ 60 kJ mol^{-1}) [34] decomposition. Such a process can be the combustion of the pyridine decomposition residues that are still present in the sample. We have also observed that at 400 °C the mass percent of the residue is less than the silver content of the compound **1**(24.5%), which confirms that a part of the AgCl end product has been evaporated [33].

In the TG–MS investigation of the gases evolved during the decomposition of compound **1** in Ar, the fragments of pyridine are seen to appear at *m*/*z* = 26 (CN), 36(C_3), 39(C_2HN), 50(C_2HN), 51(C_2H_2N), 52(C_2H_3N) and 79 (C_5H_5N) showing the loss of pyridines in the first two steps up to $\sim$ 300 °C. The *m*/*z* = 30 and *m*/*z* = 44 peaks probably belong to NO and/or CO_2/N_2O, respectively, all of which are possible oxidation products. These bands do not appear in the ESI MS of free pyridine [35], obviously because of the absence of oxygen. The intensity ratio of *m*/*z* = 28 and parent *m*/*z* 44 peaks (CO from CO_2 or N_2 from N_2O) suggests that the *m*/*z* = 44 probably belongs to CO_2 and not to N_2O [36]. The appearance of the *m*/*z* = 18 and 17 peaks (both coming from H_2O) indicates that pyridine is oxidized because the only hydrogen source can be the pyridine ligand. Since external oxygen is not provided, the source of oxygen appearing in the formed oxides, CO_2/N_2O, NO and H_2O, can only be the perchlorate. Besides, AgCl is also a product of intramolecular pyridine oxidation. But the silver chloride content of the first intermediate, compound **2** ([$Agpy_2$]ClO_4) (**DI-85**), is lower than its limit of detection by PXRD. This suggests that the intramolecular pyridine oxidation is only a side reaction, and the pyridine loss is the main. The second intermediate, ($AgClO_4$, DI-350), contains somewhat more AgCl. It is detectable, but still below 10%.

The perchlorates like potassium perchlorate oxidize carbon black between 320 and 385 °C with the formation of CO_2 and potassium perchlorate [37]. Due to the peak of *m*/*z* 44 at 321 °C, the decomposition of $AgClO_4$ at this temperature can be attributed to the oxidation of carbon residues formed in pyridine degradation in the first two decomposition steps well below 321 °C. In accordance with the literature [34], the presence of AgCl promotes the oxidation of carbon residues by $AgClO_4$. The unreacted $AgClO_4$ after the oxidation of carbon, in the presence of AgCl, decomposes as pure silver perchlorate does, with O_2 evolution (Fig. 4) somewhat above 400 °C, but still below the melting point of pure $AgClO_4$ (485 °C) [34]. The appearance of oxygen at $\sim$ 400 °C as decomposition product of compound **1** (without H_2O or CO_2 evolution) shows the lack of carbon- or hydrogen-containing materials (pyridine or degradation products) in this decomposition stage and is in agreement with the identity of the residue as pure AgCl (Suppl. Fig. 13). No formation of elementary silver, hydrochloric acid and silver oxide has been observed in any of the decomposition steps of compound **1**. It indicates that the whole chlorine content of the perchlorate group quantitatively formed silver chloride [38]. Since there was no oxygen evolution during pyridine oxidation reactions, it seems to be very probable that the redox reactions occur in the solid phase. The probability of gas-phase oxidation of the evolved pyridine by the oxygen from perchlorate is minor. The occurrence of the solid-phase oxidation can be well explained by the presence of hydrogen bonds between the pyridine α-C hydrogens and perchlorate oxygens, which can be obvious starting points of the reaction. An analogous redox reaction was seen in the thermal decomposition of the isomorphic permanganate compound (**1-MnO_4**) [17] and of [$Agpy_2$]MnO_4·0.5py as well [39] (Fig. 5).

The reaction routes found during decomposition of compound **1** are summarized in Scheme 1.

Calorimetric characteristics of compound 1

To follow the role of the oxygen content of the air flow in the decomposition process and determine the reaction heats of each stage, two series of DSC measurement were done with compound **1**, one in inert atmosphere of N_2 and another in pure oxygen (Fig. 6). The DSC curve shows that all processes of thermal degradation up to $\sim$ 200 °C in both atmospheres are followed by the endothermic heat effect corresponding to the loss and degradation of pyridine ligands. The first DSC peaks appear at 87 and 91 °C, and the reaction heat was found to be 63 and 105 kJ mol^{-1} in N_2 and O_2, respectively. Although the pyridine oxidation is only a side reaction, its rate is higher in the first decomposition step in oxygen than in nitrogen. The following endothermic peaks at 102 and 103 °C (8.361 and 9.046 kJ mol^{-1}), and at 148 and 150 °C (108.972 and 97.760 kJ mol^{-1}) in N_2 and O_2, respectively, suggest pyridine loss and melting of the solid phase. The close temperatures and heat values are indicating that the same processes take place in both gases up

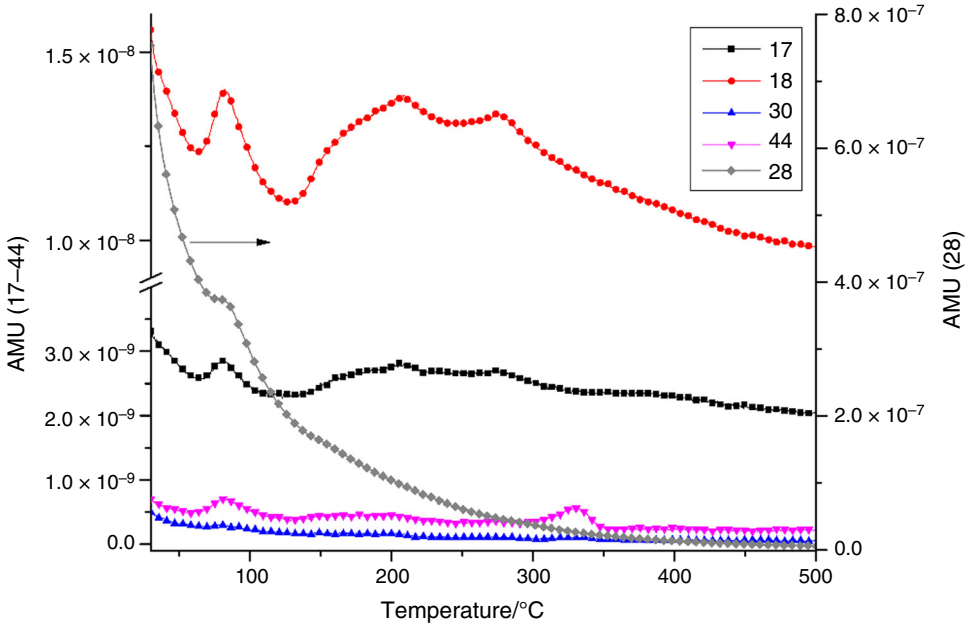

Fig. 5 TG–MS ion intensities (in arbitrary units) of the pyridine and its oxidation products (H_2O, CO_2/N_2O, CO and NO) during decomposition of compound **1** under Ar

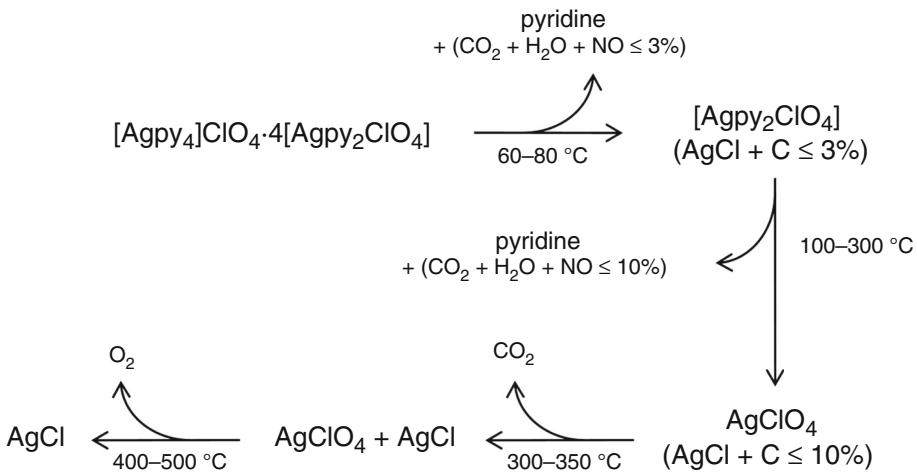

Scheme 1 Summarized decomposition route of compound **1**

to ~ 200 °C. It means that in both atmospheres, the dominant process is ligand loss, and solid-phase oxidation is minor. Above 200 °C in N_2 begins the fast oxidation of carbonaceous residues of pyridine by perchlorate. These processes are followed by high heat release. Differently, in an oxidative atmosphere, most probably the intramolecular oxidation of pyridine is hindered, but its evaporation is promoted. The sum of all heat effects up to ~ 300 °C is endothermic. To give the most probable reaction route, one has to take into account that DSC measurements are taken in crimped pans. In the case of **1** in the lid was drilled a hole for releasing the gaseous decomposition products. It means that the decomposition mechanism is different than in the case of simultaneous TG–DTA/DSC-MS measurements taken in open crucibles. In closed or partially closed pans, the decomposition occurs in a self-generated atmosphere,

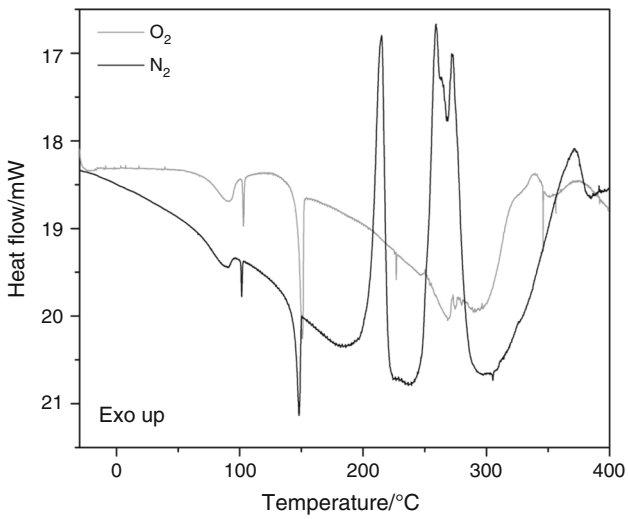

Fig. 6 DSC curves of **1** in N_2 and O_2

which is significantly changing the conditions of reaction equilibrium.

Conclusions

A simple synthetic method has been developed to prepare $4[Agpy_2]ClO_4 \cdot [Agpy_4]ClO_4$ (**1**) with low-temperature-controlled decomposition of $[Agpy_4]ClO_4$, and its detailed vibrational spectroscopic (IR, Raman and far-IR) study including factor group analysis has been performed. The compound decomposes quickly in a multistep ligand loss process with the formation of $[Agpy_2]ClO_4$ and $AgClO_4$ intermediates and AgCl as an end product. The primary ligand loss leads to the formation of $[Ag(NH_3)_2]ClO_4$ (**DI-85**), but a small amount of pyridine is removed in a redox reaction, in which perchlorate is reduced to AgCl and pyridine is oxidized into carbon or carbon dioxide, water and NO. The elementary carbon formed in this step is oxidized by $AgClO_4$ produced at higher temperature by complete ligand loss, in an AgCl–$AgClO_4$ eutectic. At high temperatures (above 400 °C), the well-known decomposition of $AgClO_4$ into AgCl and O_2 was observed.The ligand loss and degradation processes are endothermic, the redox reactions and carbon oxidation; furthermore, the $AgClO_4$ decomposition into AgCl and O_2 is exothermic processes. The amount of evolved heats was determined by DSC both in N_2 and in O_2 atmospheres. The aerial conditions have an influence on the rupture of Cl–O bond and formation of AgCl, which can control the further decomposition processes as eutectic melt-forming agent and an accelerator of $AgClO_4$ decomposition.

Acknowledgements Open access funding provided by MTA Research Centre for Natural Sciences (MTA TTK). The research within project Nos. VEKOP-2.3.2-16-2017-00013 and GINOP-2.2.1-15-2017-00084 was supported by the European Union and the State of Hungary, co-financed by the European Regional Development Fund. I. M. Szilágyi and P. Németh are grateful for the JánosBolyai Research Fellowship of the Hungarian Academy of Sciences. I. M. Szilágyi acknowledges the ÚNKP-18-4-BME-238 financial support provided by the New National Excellence Program of the Ministry of Human Capacities, Hungary. An NRDI K 124212 and an NRDI TNN_16 123631 grants are acknowledged. The research reported in this paper was supported by the Higher Education Excellence Program of the Ministry of Human Capacities in the frame of Nanotechnology and Materials Science research area of Budapest University of Technology (BME FIKP-NAT). B. BartaHolló thanks the Ministry of Education, Science and Technological Development, the Republic of Serbia for financial support; contract Grant number ON 172014.

References

1. Lozano-Torres B, Dolores Marcos M, Félix Sancenón T, Martínez-Máñez R, Rurack K. Anilinopyridine–metal complexes for the selective chromogenic sensing of cyanide anion. J Coord Chem. 2018;71(6):786–96. https://doi.org/10.1080/00958972.2018.1434719.
2. Jia PP, Ouyang RZ, Cao PH, Tong X, Zhou X, Lei T, Zhao YF, Guo N, Chang HZ, Miao YG, Zhou SA. Review: recent advances and future development of metal complexes as anticancer agents. J Coord Chem. 2017;70(13):2175–201. https://doi.org/10.1080/00958972.2017.1349313.
3. Melchior A, Tolazzi M, Polese P, Zanonato PL. Thermodynamics of complex formation of silver(I) with N-donor ligands in non-aqueous solvents. J Therm Anal Calorim. 2017;130(1):461–9. https://doi.org/10.1007/s10973-017-6289-1.
4. Habala L, Devínsky L, Egger AE. Review: metal complexes as urease inhibitors. J Coord Chem. 2018;71(7):907–40. https://doi.org/10.1080/00958972.2018.1458228.
5. Haiduc I. Nitrogen centered inverse coordination complexes. A survey of molecular topologies. J Coord Chem. 2018;71(19):3139–79. https://doi.org/10.1080/00958972.2018.1515429.
6. Del Piero S, Fedele R, Melchior A, Portanova R, Tolazzi M, Zangrando E. Solvation effects on the stability of silver(I) complexes with pyridine-containing ligands studied by thermodynamic and DFT methods. Inorg Chem. 2007;46(11):4683–91. https://doi.org/10.1021/ic070124d.
7. Di Bernardo P, Melchior A, Portanova R, Tolazzi M, Zanonato PL. Complex formation of N-donor ligands with group 11 monovalent ions. Coord Chem Rev. 2008;252(10–11):1270–85. https://doi.org/10.1016/j.ccr.2007.12.007.
8. Sajó IE, Kovács GB, Pasinszki T, Bombicz PA, May Z, Szilágyi IM, Jánosity A, Banerji KK, Kant R, Kótai L. The chemical identity of "$[Ag(py)_2]MnO_4$" organic solvent soluble oxidizing agent and new synthetic routes for the preparation of $[Ag(py)_n]XO_4$ (X = Mn, Cl, and Re, n = 2–4) complexes. J Coord Chem. 2018;71(16–18):2884–904. https://doi.org/10.1080/00958972.2018.1493464.
9. Macy R. The ternary system: silver perchlorate, pyridine and water. J Am Chem Soc. 1925;47:1031–6. https://doi.org/10.1021/ja01681a017.
10. Kótai L, Sajó I, Fodor J, Szabó P, Jakab E, Argay G, Holly S, Gacs I, Banerji KK. Reasons for and consequences of the mysterious behaviour of newly prepared hemipyridine solvate of bis(pyridine)silver(I) permanganate, $Agpy_2MnO_4$*0.5py. Transit Metal Chem. 2005;30(8):939–43. https://doi.org/10.1007/s11243-005-6231-4.
11. Schilt AA. Perchloric acid and perchlorate. Columbus: G. Frederick Smith Chemical Co.; 1979.
12. Kauffman GB, Pinnell RP. Bis(pyridine)silver(I) perchlorate. Inorg Synth. 1960;6:6–8.
13. Chen CY, Zeng JY, Lee HM. Argentophilic interaction and anionic control of supramolecular structures in simple silver pyridine complexes. Inorg Chim Acta. 2007;360(1):21–30. https://doi.org/10.1016/j.ica.2006.06.013.
14. Bowmaker GA, Effendy KCL, Skelton BW, Sukarianingsih D, White AH. Syntheses, structures and vibrational spectroscopy of some 1:2 and 1:3 adducts of silver(I) oxyanion salts with pyridine and piperidine bases containing non-coordinating 2(6)-substituents. Inorg Chim Acta. 2005;358:4342–50. https://doi.org/10.1016/j.ica.2005.04.008.
15. Dyason JC, Healy PC, Engelhardt LM, White AH. Lewis-base adducts of group 1B metal(I) compounds. XXII. Crystal structure

of 'Bis(pyridine)silver(I) Perchlorate'. Aust J Chem. 1985;38(9):1325–8. https://doi.org/10.1071/CH9851325.
16. Nilsson K, Oskarsson A. The crystal structure of tetrapyridine copper(I) perchlorate and tetrapyridine silver(I) perchlorate at 260 K. Acta Chem Scand Ser A Phys Inorg Chem. 1982;A36(7):605–10. https://doi.org/10.3891/acta.chem.scand.36a-0605.
17. Kovács GB, May NV, Bombicz PA, Klébert Sz, Németh P, Menyhárd A, Novodárszki Gy, Petrusevski V, Franguelli FP, Magyari J, Béres K, Szilágyi IM, Kótai L. An unknown component of a selective and mild oxidant: structure and oxidative ability of a double salt-type complex having unique κ^1-O-coordinated permanganate anions and three- and four-fold coordinated silver cations. RSC Adv. (**submitted to publish**)
18. Kálmán A, Párkányi L, Argay Gy. Classification of the isostructurality of organic molecules in the crystalline state. Acta Crystallogr Sect B. 1993;49:1039–49. https://doi.org/10.1107/S010876819300610X.
19. Spek AL. Single crystal structure validation with the program PLATON. J Appl Crystallogr. 2003;36:7–13. https://doi.org/10.1107/S0021889802022112.
20. van der Bondi A. Waals volume and radii. J Phys Chem. 1964;68:441. https://doi.org/10.1021/j100785a001.
21. Schmidbaur H, Schier A. Argentophilic interactions. Angew Chem Int Ed. 2015;54:746–84. https://doi.org/10.1002/anie.201405936.
22. Bayler A, Schier A, Bowmaker GA, Schmidbaur H. Gold is smaller than silver. Crystal structures of [Bis(trimesitylphosphine)gold(I)] and [Bis(trimesitylphosphine)silver(I)] tetrafluoroborate. J Am Chem Soc. 1996;118:7006. https://doi.org/10.1021/ja961363v.
23. Nyburg SC, Faerman CH. A revision of van der Waals atomic radii for molecular crystals: N, O, F, S, Cl, Se, Br and I bonded to carbon. Acta Crystallogr Sect. 1985;B41:274. https://doi.org/10.1107/S0108768185002129.
24. Petrusevski V, Trencevski KA. Tensorial approach to the description of molecular distortions I. Tetrahedral molecules. Croat Chem Acta. 1986;59(4):867–81.
25. Petrusevski V, Soptrayanov B. Description of molecular distortions II. Intensities of the symmetric stretching bands of tetrahedral molecules. J Mol Struct. 1988;175:349–54. https://doi.org/10.1016/S0022-2860(98)80101-4.
26. Buck RP, Singhadeja S, Rogers LB. Ultraviolet absorption spectra of some inorganic ions in aqueous solutions. Anal Chem. 1954;26(7):1241–2. https://doi.org/10.1021/ac60091a051.
27. Bando Y, Tagakura S. The electronic structure and spectrum of the silver(I)perchlorate-pyridine complex. Theor Chim Acta. 1968;9:210–21. https://doi.org/10.1007/BF00526600.
28. Boopalachandran P, Laane J. Ultraviolet absorption spectra of pyridine-d0 and -d5 and their ring-bending potential energy function in the S1(n, π*) state. Chem Phys Lett. 2008;462:178–82. https://doi.org/10.1016/j.cplett.2008.07.080.
29. Nockemann P, Meyer G. $[Ag(NH_3)_2]ClO_4$: Kristallstrukturen, Phasenumwandlung, Schwingungsspektren. Z Anorg Allgem Chem. 2002;628:1636–40. https://doi.org/10.1002/1521-3749(200207)628:7%3c1636:AID-ZAAC1636%3e3.0.CO;2-M.
30. Miller FA, Wilkins CH. Infrared spectra and characteristics frequencies of inorganic ions. Anal Chem. 1952;24(8):1253–94. https://doi.org/10.1021/ac60068a007.
31. Kótai L, Horváth T, Szentmihályi K, Keszler Á. Evidence-forquasi-intramolecular acid-base reactions in solutions of transition metal ammine complexes. Transit Metal Chem. 2000;25(3):293–4. https://doi.org/10.1023/A:1007068408687.
32. Kótai L, Gács I, Kazinczy B, Sajó IE, Sreedhar B. Quasi-intramolecular acid-base reactions in aqueous solutions of metal-complexes of basic ligands I. Generalized theoretical considerations on the deammoniation of $[ML_m]X_n$ type ammonia complexes. Transit Metal Chem. 2003;28(3):292–5. https://doi.org/10.1023/A:1022908030402.
33. Visnapuu A, Jensen JW. Composition and properties of vapors over molten silver chloride. J Less-Common Met. 1970;20:141–8. https://doi.org/10.1016/0022-5088(70)90099-8.
34. Solymosi F. The thermal stability and some physical properties of silver chlorite, chlorate and perchlorate. Z Phys Chem Neue Folge. 1968;57:1–18. https://doi.org/10.1524/zpch.1968.57.1_2.001.
35. Lifshitz C. Time-dependent mass spectra and breakdown graphs. 2. The kinetic shift in pyridine. J Phys Chem. 1982;86(5):606–12. https://doi.org/10.1021/j100394a006.
36. Kocsis T, Magyari J, Sajó IE, Pasinszki T, Homonnay Z, Szilágyi IM, Farkas A, May Z, Effenberger H, Szakáll S, Pawar RP, Kótai L. Evidence of quasi-intramolecular redox reactions during thermal decomposition of ammonium hydroxodisulfitoferriate(III), $(NH_4)_2[Fe(OH)(SO_3)_2]\cdot H_2O$. J Therm Anal Calorim. 2018;132:493–502. https://doi.org/10.1007/s10973-017-6901-4.
37. Patai S, Hoffmann E. The oxidation of carbon black by solid potassium perchlorate. J Am Chem Soc. 1950;72:5098–101. https://doi.org/10.1021/ja01167a078.
38. Markowitz MM. A basis for the prediction of the thermal decomposition products of metal perchlorates. J Inorg Nucl Chem. 1963;25:407–14. https://doi.org/10.1016/0022-1902(63)80191-8.
39. Kotai L, Fodor J, Jakab E, Sajo I, Szabo P, Lonyi F, Valyon J, Gacs I, Argay G, Banerji K. A thermally induced low-temperature intramolecular redox reaction of bis(pyridine)silver(I) permanganate and its hemipyridine solvate. Trans Metal Chem. 2006;31(1):30–4. https://doi.org/10.1007/s11243-005-6322-2.